



OPEN

Visible-light induced degradation of diphenyl urea and polyethylene using polythiophene decorated CuFe_2O_4 nanohybrids

Ufana Riaz^{1,2✉}, Shayista Gaffar², Kristen Hauser¹ & Fei Yan¹

The present work reports facile synthesis of CuFe_2O_4 nanoparticles via co-precipitation method and formulation of its nanohybrids with polythiophene (PTh). The structural and morphological properties were investigated using fourier transform infrared spectroscopy (FT-IR), X-ray diffraction (XRD), scanning electron microscopy coupled with energy dispersive spectra (SEM-EDS) and UV-Vis spectroscopy. The band gap was found to decrease with increase in the loading of PTh and was found to be 2.52 eV for 1-PTh/ CuFe_2O_4 , 2.15 eV for 3-PTh/ CuFe_2O_4 and 1.89 eV for 5-PTh/ CuFe_2O_4 . The nanohybrids were utilized as photocatalysts for visible light induced degradation of diphenyl urea. Diphenyl urea showed 65% degradation using 150 mg catalyst within 120 min. Polyethylene (PE) was also degraded using these nanohybrids under visible light as well as microwave irradiation to compare its catalytic efficiency under both conditions. Almost 50% of PE was degraded under microwave and 22% under visible light irradiation using 5-PTh/ CuFe_2O_4 . The degraded diphenyl urea fragments were analyzed using LCMS and a tentative mechanism of degradation was proposed.

Urea is the most common nitrogen fertilizer used in agriculture worldwide and is generated in excess of 140 million tons annually¹. About 650 tons of wastewater is discharged per day containing 0.5–2 wt% urea which is harmful to natural streams because it encourages the growth of algae and hydrolyzes slowly, releasing ammonia that is toxic to fish^{2–4}. Besides this, many urea derivatives such as phenyl and sulfonyl urea are widely adopted as herbicides for the control of broad-leaved weeds and wild grasses in many agricultural crops. These compounds serve as persistent water pollutants due to their fairly high water solubility and relative photochemical stability. Likewise, plastic pollution has become a global problem and according to the US EPA (United States Environmental Protection Agency) more than 200 tons of plastic is produced annually⁵. Micro-plastics (MPs) (plastic materials with < 5 nm) that are directly discharged into the environment can build up in the stomach, induce blockage, inflammation in many organs and also produce genotoxicity^{6–9}. The treatment of urea wastewater via biological^{5,6}, enzymatic¹⁰ and electrochemical approaches have been attempted by several authors, while very few studies have been carried out on the degradation of plastics, including the bio/photocatalytic degradation of polyethylene polymers by *Zalerion maritimum*¹¹ TiO_2 nanotubes¹², ZnO ¹³, N-doped TiO_2 ^{14,15}, and Pt/ ZnO ^{16,17}.

Lately, the photocatalytic properties of spinel ferrites have been widely reported for oxidative dehydration of hydrocarbons¹⁸, decomposition of alcohols and hydrogen peroxide¹⁹, oxidation of carbon monoxide²⁰, and degradation of dyes^{21–26}. Due to the alternation of Fe^{+3} and Fe^{+2} states, ferrites have been reported to exhibit remarkable structural stability as well as catalytic activity^{22,23}. Conducting polymers such as polycarbazole (PCz)²², poly(o-phenylenediamine) (POPD)²⁴, polypyrrole (PPy)²⁶, polyaniline (PANI)²⁷, polythiophene (PTh)²⁸, are widely known to act as sensitizers and reduce the band gap of the metal oxides. Lately few authors have reported the degradation of polymers using spinels^{29,30}. However, no work has been reported on the utilization of CuFe_2O_4 in the degradation of diphenyl urea/plastics. Hence, with a view to explore the photocatalytic efficiency of conducting polymer-sensitized nanohybrids in the degradation of plastics as well as diphenyl urea which are seldom investigated persistent organic pollutants, we have synthesized magnetic CuFe_2O_4 nanoparticles and formulated its nanohybrids using different loadings of PTh. The synthesized nanomaterials were characterized for their spectral, thermal, and morphological properties. CuFe_2O_4 and PTh/ CuFe_2O_4 nanohybrids were chosen to evaluate the degradation efficiency of diphenyl urea and PE. The degradation of diphenyl urea was systematically

¹Department of Chemistry and Biochemistry, North Carolina Central University, Durham, NC 27707, USA. ²Materials Research Laboratory, Department of Chemistry, Jamia Millia Islamia, New Delhi 110025, India. ✉email: ufana2002@yahoo.co.in; uriaz@nccu.edu

investigated by varying the effect of urea as well as the nanohybrid concentration. The reusability of CuFe_2O_4 and $\text{CuFe}_2\text{O}_4/\text{PTh}$ nanohybrids were evaluated and the mechanism of degradation was proposed based on the radical scavenging experiments and LCMS studies. The degradation of PE was studied under visible light irradiation as well as microwave irradiation and the degradation was confirmed via weight loss studies and IR analysis.

Materials and methods

Materials. Cupric chloride (CuCl_2), (Merck, India), ferric chloride (FeCl_3) (Sigma Aldrich, USA), Ammonia (Sigma Aldrich, USA), thiophene (Sigma Aldrich, USA), tert-butanol (TBA) (Merck, India), disodium sulfate (Na_2SO_4) (Sigma Aldrich, USA), ethylene diamine tetra acetate (EDTA) (Sigma Aldrich, USA), sodium nitrate (Sigma Aldrich, USA), ethanol (Merck, India), chloroform (Merck, India), were used without further purification. Urea ($\text{CH}_4\text{N}_2\text{O}$) (molar mass 60.06 g/mol) (Merck, India) was used as received.

Synthesis of CuFe_2O_4 nanoparticles. Cupric chloride (CuCl_2) (2 g) and FeCl_3 (4 g) were dissolved in distilled water (50 ml) under vigorous magnetic stirring at room temperature (25 °C) for 30 min. A solution of ammonia (3 M, 25 ml) was added drop-wise into the above mixture under constant stirring on a magnetic stirrer for 1 h to attain a pH level of 11–12. The solution was further heated at 80 °C for 2 h and the product was cooled to room temperature after 1 h. The precipitate was collected via centrifugation for 5 min at 300 rpm, washed with ethanol to remove unreacted precursors and then dried in vacuum oven at 120 °C for 12 h. After drying, the precipitate was subjected to calcination at 500 °C for 3 h in a muffle furnace to obtain CuFe_2O_4 nanoparticles.

Synthesis of PTh modified CuFe_2O_4 nanohybrids. CuFe_2O_4 nanoparticles (1 g) were dispersed in a solution of $\text{CHCl}_3:\text{H}_2\text{O}$ mixture (30 ml/30 ml v/v) in a 150 ml conical flask and thiophene monomer (0.01 ml) was added to the same flask. The reaction mixture was sonicated at 25 °C on an ultrasonic bath (30 kHz) for 30 min. Ferric chloride (0.019 g) (thiophene is to FeCl_3 ratio 1:1) dissolved in CHCl_3 (30 ml) was then added drop wise to the above reaction mixture and subjected to further sonication for 4 h. The obtained nanohybrid was filtered, washed several times with distilled water and dried in vacuum oven for 24 h at 80 °C. Based on the weight ratios of the ferrite/monomer taken, the nanohybrids were designated as 1-PTh/ CuFe_2O_4 , 3-PTh/ CuFe_2O_4 and 5-PTh/ CuFe_2O_4 .

Characterization. *Morphological analysis.* The XRD profiles were recorded on Philips PW 3710 powder X-ray diffractometer using Ni-filtered $\text{Cu-K}\alpha$ radiation. The morphology and microstructures of the synthesized samples were investigated by field emission-scanning electron microscopy (FE-SEM) (FEI, Nova nano SEM 30 KVA, Germany).

Spectral analysis. The IR spectra were recorded on the FTIR spectrophotometer (Perkin Elmer, USA) in the form of powder. The UV–Vis diffuse reflectance (UV-DRS) spectra were captured on a PerkinElmer Lambda 30 spectrophotometer using BaSO_4 as a reference.

Visible light induced degradation studies. Degradation experiments were carried out using xenon lamp light source (500 W, CEL-S500F, Beijing, China) (spectrum provided in supporting information as Fig. S1). Approximately 150 mg of the catalyst was dispersed in diphenyl urea solution (300 ml) and was sonicated for 10 min. The suspension was then kept under dark conditions to stabilize the adsorption–desorption equilibrium between the diphenyl urea solution and catalyst. The diphenyl urea solution was exposed to visible irradiation for 120 min and aliquots of solution (3 ml) were taken out at regular intervals of 0, 20, 40, 60, 80, 100 and 120 min. The UV spectrum of the diphenyl urea was recorded using UV–Vis spectrophotometer model Perkin-Elmer Lambda 30 at λ_{max} value of 250 nm.

Scavenging experiments for analysis of radical responsible for diphenyl urea degradation. The reactive species responsible for the degradation of diphenyl urea were investigated as per method reported in our previous studies using 5 mM of scavengers namely tert-butanol (TBA) (for $\cdot\text{OH}$ radical detection), sodium nitrate (for $\text{O}_2^{\cdot-}$ radical detection), ethylene diamine tetra acetate (EDTA) (for hole (h^+) detection) and disodium sulfate (Na_2SO_4) (for electron (e^-) detection)^{31,32}. To study the impact of the scavengers on the degradation rate, the scavengers were added one at a time to the urea solution containing the catalyst (50 mg).

Recyclability tests for urea degradation. The reusability of CuFe_2O_4 and PTh/ CuFe_2O_4 nanohybrids were evaluated for the degradation process up to four cycles. The nanohybrids CuFe_2O_4 and $\text{CuFe}_2\text{O}_4/\text{PTh}$ nanohybrids were collected after completion of each cycle, washed with distilled water and dried under vacuum oven at 60 °C for 6 h. The obtained catalysts were reused in the next cycle and the process was repeated three times.

Results and discussion

Structural confirmation of CuFe_2O_4 and $\text{CuFe}_2\text{O}_4/\text{PTh}$ nanohybrids via XRD and SEM studies. The XRD profile of CuFe_2O_4 , Fig. 1, revealed diffraction peaks at $2\theta = 32.14^\circ$, 39.42° , 41.82° , 46.04° with Miller indices (220), (311), (222), and (400) respectively, which matched very well with the characteristic peaks of CuFe_2O_4 and with the space group of $\text{Fd}3\text{m}$ ³³. The peaks matched well with the cubic phase of CuFe_2O_4 as per JCPDS card no 34-0425. The reflection peaks with miller indices (220) and (400) were found to be most intense and were associated with the characteristic peaks of spinel phase. The reflection peak patterns were coherent with single phase cubic structure confirming the solubility of Cu^{2+} into Fe_3O_4 and formation of well-crystallized

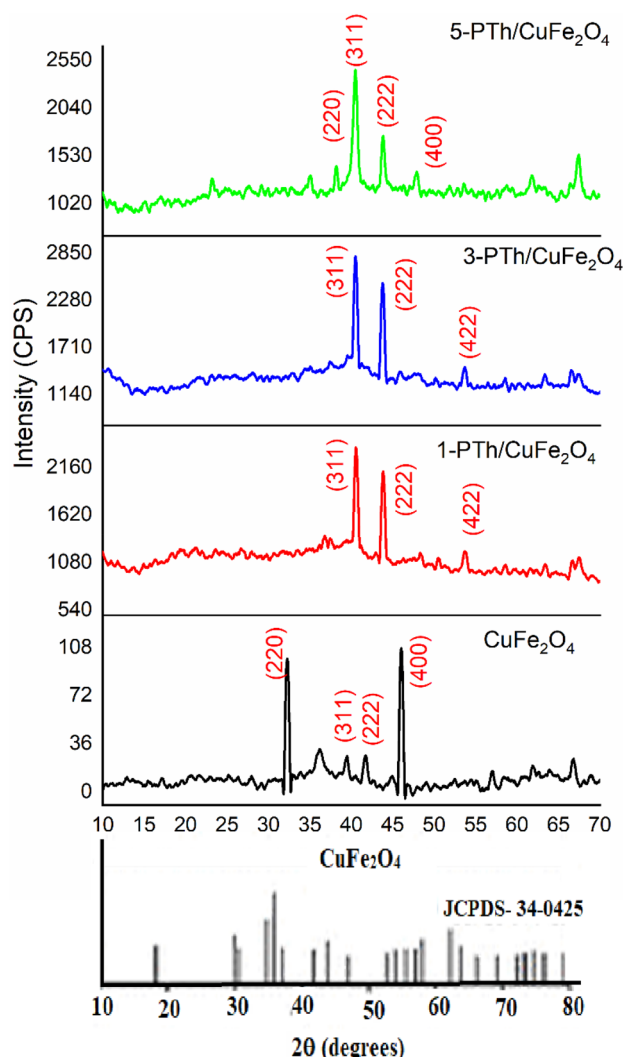


Figure 1. XRD profile of CuFe_2O_4 , 1-PTh/ CuFe_2O_4 , 3-PTh/ CuFe_2O_4 , and 5-PTh/ CuFe_2O_4 .

nanostructure^{33,34}. The average grain size was estimated to be 45 Å using the Debye–Scherrer formula³⁵. The nanohybrids revealed prominent reflection peaks corresponding to CuFe_2O_4 at 40.6° and 43.8° with Miller indices (311) and (222). The peaks were found to be more prominent than the ones with Miller indices (220) and (400) presumably due to the change in the orientation of the planes upon loading of PTh. Since no other peaks associated with the presence of PTh were noticed, the nanohybrids were confirmed to be encapsulated with the polymer. The crystallinity of CuFe_2O_4 spinel was noticed to remain intact even upon loading of the polymer up to 5% in the nanohybrids. The encapsulation of the spinel by the polymer was further confirmed by the morphological studies discussed in the proceeding section.

SEM analysis. The morphological studies of as prepared CuFe_2O_4 nanoparticles and CuFe_2O_4 /PTh nanohybrids were investigated by SEM, Fig. 2a–d. The SEM image of CuFe_2O_4 , Fig. 2a, exhibited the formation of bright distorted cubes. The SEM of 1-PTh/ CuFe_2O_4 nanohybrid, Fig. 2b, showed granular morphology, while the SEM of 3-PTh/ CuFe_2O_4 , Fig. 2c, revealed the presence of cubical clusters of CuFe_2O_4 and granular particles which were associated with PTh. The SEM of 5-PTh/ CuFe_2O_4 , Fig. 2d, showed presence of distorted bright cubes enclosed with PTh dark granular aggregates. There was slight variation noticed in the particle sizes upon increasing the loading of PTh in CuFe_2O_4 . Thus, it can be inferred that the nanohybrids revealed encapsulation of CuFe_2O_4 with spherical PTh particles forming dense dark agglomerates. The elemental composition of CuFe_2O_4 and CuFe_2O_4 /PTh nanohybrids was determined by EDS analysis and showed the presence of Cu, Fe and O with stoichiometric values matching that of CuFe_2O_4 composition (Fig. 2a), whereas the EDS spectrum of CuFe_2O_4 /PTh nanohybrids showed the presence of C and S in addition to Cu, Fe and O, Fig. 2b–d.

IR studies. The IR spectra of CuFe_2O_4 and its nanohybrids CuFe_2O_4 /PTh were also studied (given in supporting information as Fig. S2). The IR spectrum of CuFe_2O_4 showed OH stretching vibration peak at 3123 cm^{-1} correlated to the presence of adsorbed water molecules. The peak at 1215 cm^{-1} was correlated Fe–Cu bond

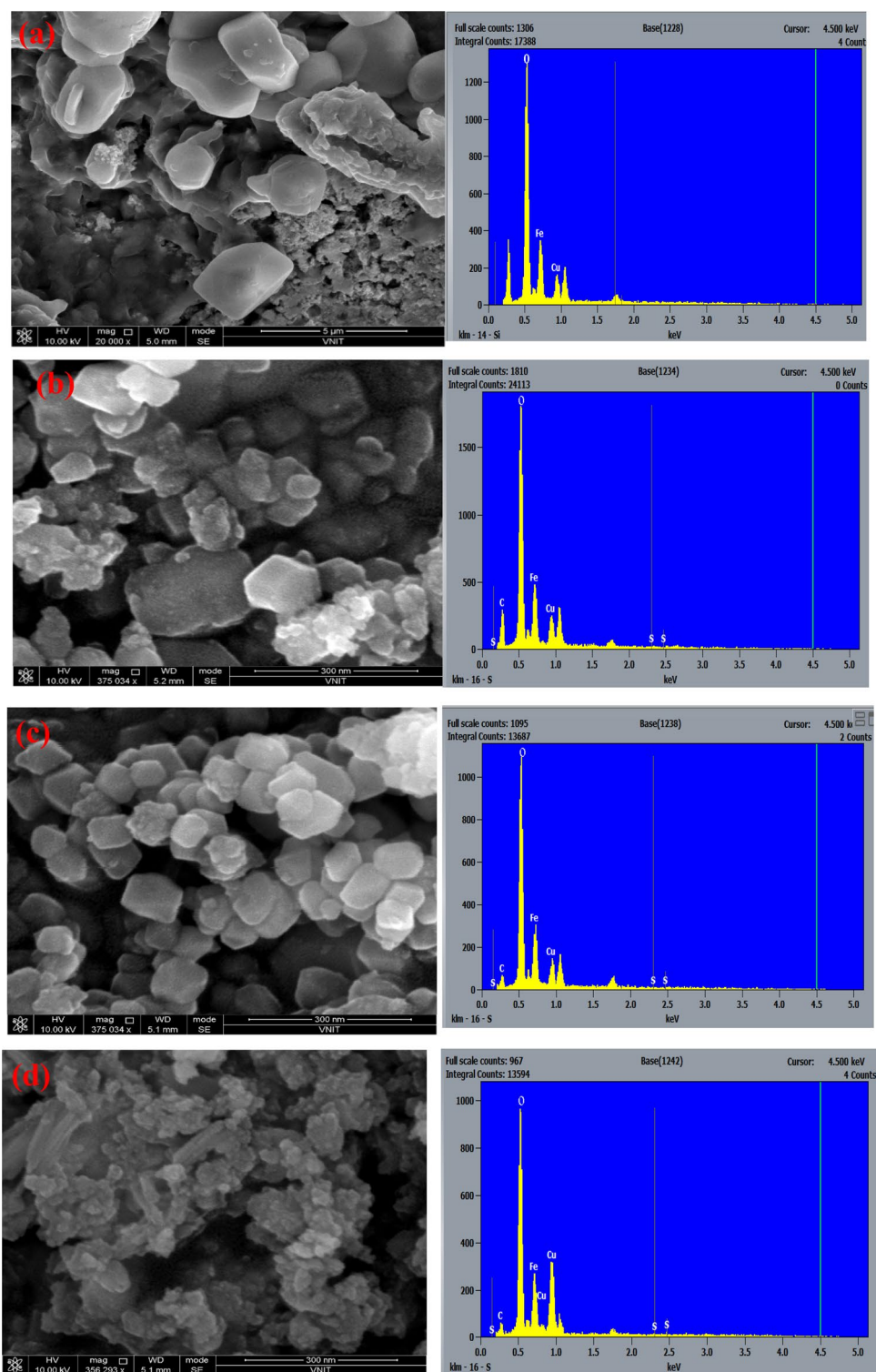


Figure 2. SEM image of (a) CuFe_2O_4 (b) 1-Th/ CuFe_2O_4 (c) 3-PTh/ CuFe_2O_4 (d) 5-PTh/ CuFe_2O_4 .

stretching vibration mode, while the peaks related to the Cu–OH bond vibration were noticed at 1069 cm^{-1} . The peak related to Fe–O stretching was noticed at 789 cm^{-1} , whereas peaks at 550 cm^{-1} , and 486 cm^{-1} were correlated to the stretching vibrations of Cu–O. The presence of the above peaks confirmed the formation of CuFe_2O_4 ^{23,36}. The IR spectrum of PTh/ CuFe_2O_4 nanohybrids showed a peak at 3121 cm^{-1} attributed to the O–H stretching vibration, while the peak at 1739 cm^{-1} was associated with the O–H bending vibrations of absorbed water molecules. The peaks at 1607 cm^{-1} and 1511 cm^{-1} was correlated to the C=C stretching vibrations in the thiophene ring molecules. The peak at 1215 cm^{-1} was assigned to the C–H bending vibrations. The characteristic

peaks at 1117 cm^{-1} and 879 cm^{-1} in IR spectrum of nanohybrids were assigned to the C–S stretching vibrations. The absorption band at 788 cm^{-1} was associated with C–H out of plane stretching vibrations and C–H plane deformation modes of PTh²⁸. The peaks at 571 cm^{-1} was also observed due to ring deformation of PTh. The presence of the peaks related to spinel as well as the polymer confirmed the formation of CuFe_2O_4 and the presence of PTh in $\text{CuFe}_2\text{O}_4/\text{PTh}$ nanohybrids.

UV analysis and confirmation of band gap. Ferrites exhibit photocatalytic activity by the absorption of visible light, which leads to the transfer of electrons from the valence band to the conduction band, creating electrons and holes. CuFe_2O_4 showed an absorption edge of around 450 nm, while the nanohybrids revealed shift in the absorption edge to 550 nm and higher with increase in the PTh loading to 5% (given in supporting information as Fig. S3). Hence, it can be concluded that the nanohybrids can efficiently absorb the light in the visible region. The Kubelka–Munk equation was applied to calculate the optical band gap^{31,32,36}. The band gap values were found to be 2.74 eV for CuFe_2O_4 , 2.52 eV for 1-PTh/ CuFe_2O_4 , 2.15 eV for 3-PTh/ CuFe_2O_4 , 1.89 eV for 5-PTh/ CuFe_2O_4 (given in supporting information as Fig. S4a–d). The band gap of CuFe_2O_4 showed a consistent decrease with an increase in the amount of PTh in the CuFe_2O_4 and was suitable for degrading diphenyl urea under visible light as discussed in the proceeding section.

Effect of urea concentration and photocatalyst concentration on degradation. Degradation of diphenyl urea was performed by visible light irradiation for a period of 120 min and was examined by UV–Vis spectroscopy. To study the effect of urea concentration, 20 ppm, 40 ppm and 60 ppm solutions were taken along with 50 mg of the photocatalyst and exposed to visible light irradiation for a period of 120 min as depicted in Fig. 3a. Almost 35% degradation of 20 ppm diphenyl urea solution was achieved in 120 min using 50 mg CuFe_2O_4 , and 29% degradation was attained for 40 ppm solution using the same amount of the photocatalyst. The 60 ppm solution showed 26% degradation efficiency within 120 min. The rate constant (k) values for 20 ppm, 40 ppm and 60 ppm degradation were calculated to be 0.0036 min^{-1} , 0.0029 min^{-1} and 0.0026 min^{-1} respectively (given in supporting information as Fig. S5a–d). The nanohybrid 1-PTh/ CuFe_2O_4 showed 30% degradation of 60 ppm solution within a span of 120 min, while almost 40% and 33% degradation was noticed for 20 ppm and 40 ppm diphenyl urea solutions respectively, Fig. 3a. The k values for 20 ppm, 40 ppm and 60 ppm degradation were found to be 0.0044 min^{-1} , 0.0033 min^{-1} and 0.0031 min^{-1} respectively (given in supporting information as Fig. S5a–d). The nanohybrids 3-PTh/ CuFe_2O_4 exhibited 49% degradation for 20 ppm diphenyl urea solution; while around 40% degradation of 40 ppm diphenyl urea solution was achieved in 120 min and 34% for 60 ppm solution. The rate constant values for 20 ppm, 40 ppm and 60 ppm were found to be 0.0058 min^{-1} , 0.0043 min^{-1} and 0.0037 min^{-1} respectively. The nanohybrids 5-PTh/ CuFe_2O_4 revealed of 57%, 47% and 41% degradation of 20 ppm, 40 ppm and 60 ppm urea solutions and the k values were observed to be 0.0072 min^{-1} , 0.0055 min^{-1} and 0.0046 min^{-1} respectively. Among the nanohybrids, 5-PTh/ CuFe_2O_4 showed highest degradation efficiency of 57% within 120 min for 20 ppm diphenyl urea solution.

To study the effect of catalyst concentration, CuFe_2O_4 and PTh/ CuFe_2O_4 nanohybrids were taken as 50 mg, 100 mg and 150 mg for degradation of 60 ppm urea solution and are depicted in Fig. 3b. With the increase in catalyst concentration, the degradation efficiency was found to increase rapidly. For CuFe_2O_4 , the degradation was observed to be 26%, 42% and 50% using 50 mg, 100 mg and 150 mg of the photocatalyst respectively. The k values were noticed to be 0.0026 min^{-1} , 0.0046 min^{-1} and 0.0055 min^{-1} respectively, (given in supporting information as Fig. S6a–d). Similarly, 1-PTh/ CuFe_2O_4 , exhibited 30%, 46% and 54% degradation with the increase in the concentration of the photocatalyst. The k values were found to be 0.0031 min^{-1} , 0.0052 min^{-1} , and 0.0064 min^{-1} . The nanohybrid 3-PTh/ CuFe_2O_4 showed 34% degradation in presence of 50 mg photocatalyst, while almost 58% degradation was attained using 150 mg photocatalyst and 51% using 100 mg catalyst. The k values were noticed to be 0.0037 min^{-1} , 0.0059 min^{-1} and 0.0074 min^{-1} respectively for 50 mg, 100 mg and 150 mg photo catalysts (given in supporting information as Fig. S6a–d). Likewise, the nanohybrid 5-PTh/ CuFe_2O_4 showed 41% degradation in presence of 50 mg photocatalyst, while almost 54% degradation was attained using 100 mg photocatalyst and 65% using 150 mg catalyst. The k values were noticed to be 0.0046 min^{-1} , 0.0065 min^{-1} and 0.0088 min^{-1} respectively for 50 mg, 100 mg and 150 mg photocatalysts.

Radical scavenging experiments. Radical trapping experiments were carried out to identify the primary reactive oxidative species involved in the photo degradation of the diphenyl urea in order to investigate the mechanism of photocatalysis in presence of CuFe_2O_4 and $\text{CuFe}_2\text{O}_4/\text{PTh}$ nanohybrids. Different scavengers sodium sulfate (Na_2SO_4) (e^- scavenger) (5 ml, 5 Mm), ethylene diamine tetra acetic acid (EDTA) (h^+ scavenger) (5 ml 5 Mm), and t-butyl alcohol (t-BuOH) (OH^\bullet scavenger) (5 ml, 5 Mm) were added into urea solution and exposed to visible irradiation for 120 min in presence of CuFe_2O_4 and its nanohybrids, Fig. 4. The spinel CuFe_2O_4 , in presence of EDTA, showed a decrease in the degradation efficiency of urea to 33%, while in presence of Na_2SO_4 , the degradation efficiency decreased to 32%. However, in presence of t-BuOH, the degradation efficiency was noticed to be 10% confirming the generation of OH^\bullet radicals as the major active species. For 1-PTh/ CuFe_2O_4 , the degradation efficiency was observed to be 30% in presence of EDTA and 20%, 14% for Na_2SO_4 and t-BuOH respectively.

Similarly, for 3-PTh/ CuFe_2O_4 , the degradation efficiency was reduced to 40% and 35% upon addition of EDTA and Na_2SO_4 respectively and 15% upon addition of t-BuOH. The nanohybrid, 5-PTh/ CuFe_2O_4 , revealed a degradation efficiency of 51% and 45% in presence of EDTA and Na_2SO_4 respectively and 10% in presence of t-BuOH. The reduction in the degradation rate in presence of t-BuOH in all cases confirmed that OH^\bullet radicals were the main active radical species as compared to e^- and h^+ involved in the photocatalytic degradation of diphenyl urea using CuFe_2O_4 and PTh/ CuFe_2O_4 as photocatalysts. The visible light induced degradation of diphenyl urea

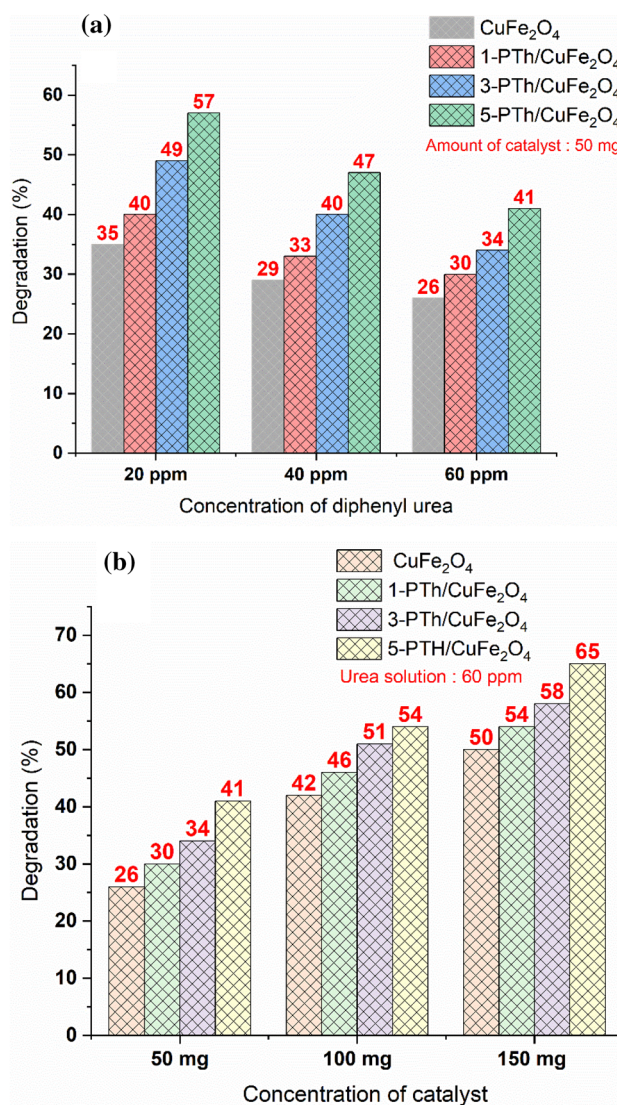


Figure 3. (a) Effect of diphenyl urea concentration (b) Effect of photocatalyst concentration on the degradation behavior of the pollutant.

using CuFe₂O₄ and PTh/CuFe₂O₄ nanohybrids generate radicals which lead to the excitation of electrons from the valence band to the conduction band and PTh acts as a sensitizer to promote electrons in the conduction band of CuFe₂O₄ creating holes (h⁺) in the VB of the later. As confirmed from the radical scavenging studies, the generation of hydroxyl radicals (·OH), causes degradation of diphenyl urea. The LCMS study (given in supporting information as Fig. S7) of the degraded fragments of diphenyl urea was used to propose the tentative degradation pathway of diphenyl urea as shown in Fig. 5. The diphenyl urea parent molecule upon exposure to hydroxyl radical fragmented to [(cyclohexa-1,4-dien-1-yl) amino] methanediol (M1) (m/z 141) which further fragmented to (2E)-N-hydroxypent-2-en-2-amine (M1) (m/z 100), urea (M3) (m/z 60) and ethenol (M4) (m/z 44).

Recyclability test. The recyclability tests, Fig. 6 showed that CuFe₂O₄ and 5% PTh-CuFe₂O₄ taken as 50 mg revealed 35% and 60% degradation of 20 ppm urea solution exhibiting high catalytic activity even after four cycles which confirmed their excellent reusability as well as stability. Therefore, 5% PTh-CuFe₂O₄ could be considered as a potential catalyst in wastewater treatment due to its fairly high reusability feature.

Comparison of visible light and microwave-assisted degradation of polyethylene. Polyethylene films (PE) were cut into strips (1 cm × 1 cm) and were subjected to visible light induced degradation using a solution of (water/DMSO) solvent. Similarly, for microwave induced degradation, the solution containing the films was degraded under microwave irradiation (Ladd Research Microwave oven) using 150 mg of CuFe₂O₄ as well as PTh/CuFe₂O₄ as catalyst and the results are shown in Fig. 7a and b.

The IR studies reveal that a major shift as well as disappearance of the peaks was observed upon photocatalytic degradation of the PE films in presence of PTh/CuFe₂O₄ as catalyst. The IR peaks of PE film before degradation

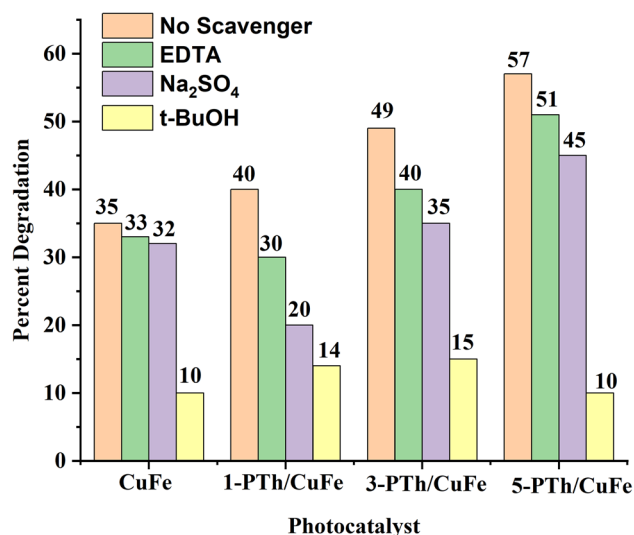


Figure 4. Effect of addition of radical scavenger on CuFe₂O₄, PTh/CuFe₂O₄ nano hybrids.

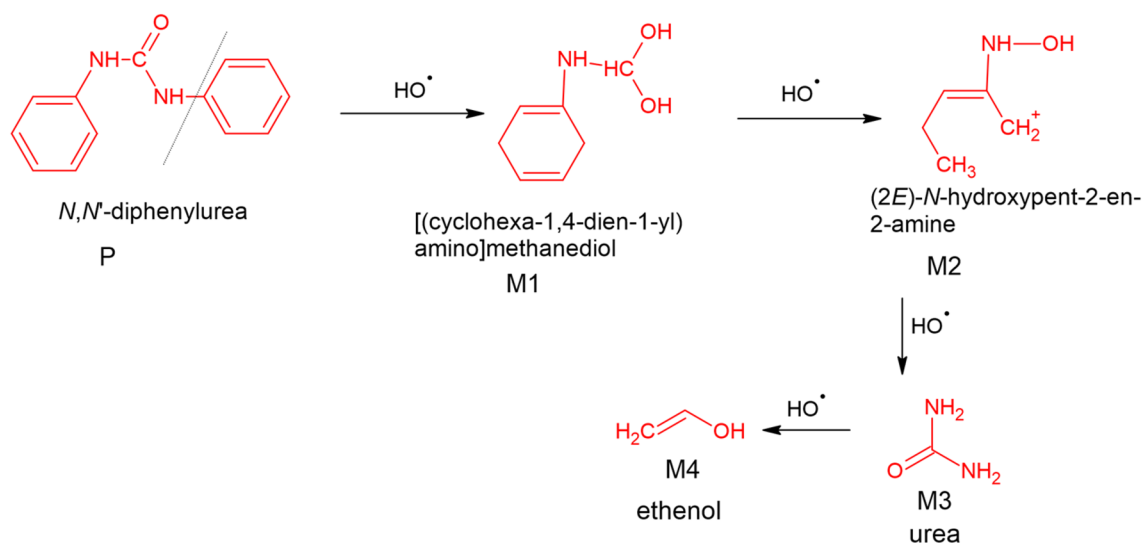


Figure 5. Mechanism of degradation of Diphenyl urea.

were noticed at 2914 cm⁻¹, 2845 cm⁻¹, 1465 cm⁻¹, 1370 cm⁻¹, 719 cm⁻¹³⁷. Upon exposure to microwave irradiation with photocatalyst for 5 h, the peaks were found to show a major shift. A shift in peaks at 1466 cm⁻¹, 1370 cm⁻¹ was observed towards 1600 cm⁻¹. The initial weight of PE was found to be 0.004 g, but after degradation decreased appreciably as shown in Table 1. The degradation was observed to be 10% using CuFe₂O₄ in presence of visible light and 28% under microwave irradiation. The degradation of PE films was found to be highest using 5-PTh/CuFe₂O₄ which was noticed to be almost 50% under microwave irradiation. It can thus be concluded that the nano hybrids could be effectively used to degrade polymers under microwave irradiation.

Conclusion

CuFe₂O₄ and PTh/CuFe₂O₄ nano hybrids were successfully prepared and characterized for their spectral as well as morphological properties. The XRD analysis confirmed the formation of CuFe₂O₄ spinel with cubic phase which undergoes encapsulation upon loading of PTh. The UV-DRS studies showed appreciable reduction in band gap values upon modification with PTh which confirmed that the nano hybrids could effectively be used for visible-light-induced photocatalysis. The visible-light induced photocatalytic degradation of diphenyl urea was carried out for 120 min, while microwave-assisted as well as visible light induced catalytic degradation of PE films was carried out for 5 h. For the visible light-induced degradation of diphenyl urea, the kinetics fitted the first-order model and was found to be 57% for the 20 ppm solution using 5-PTh/CuFe₂O₄ nano hybrid. The

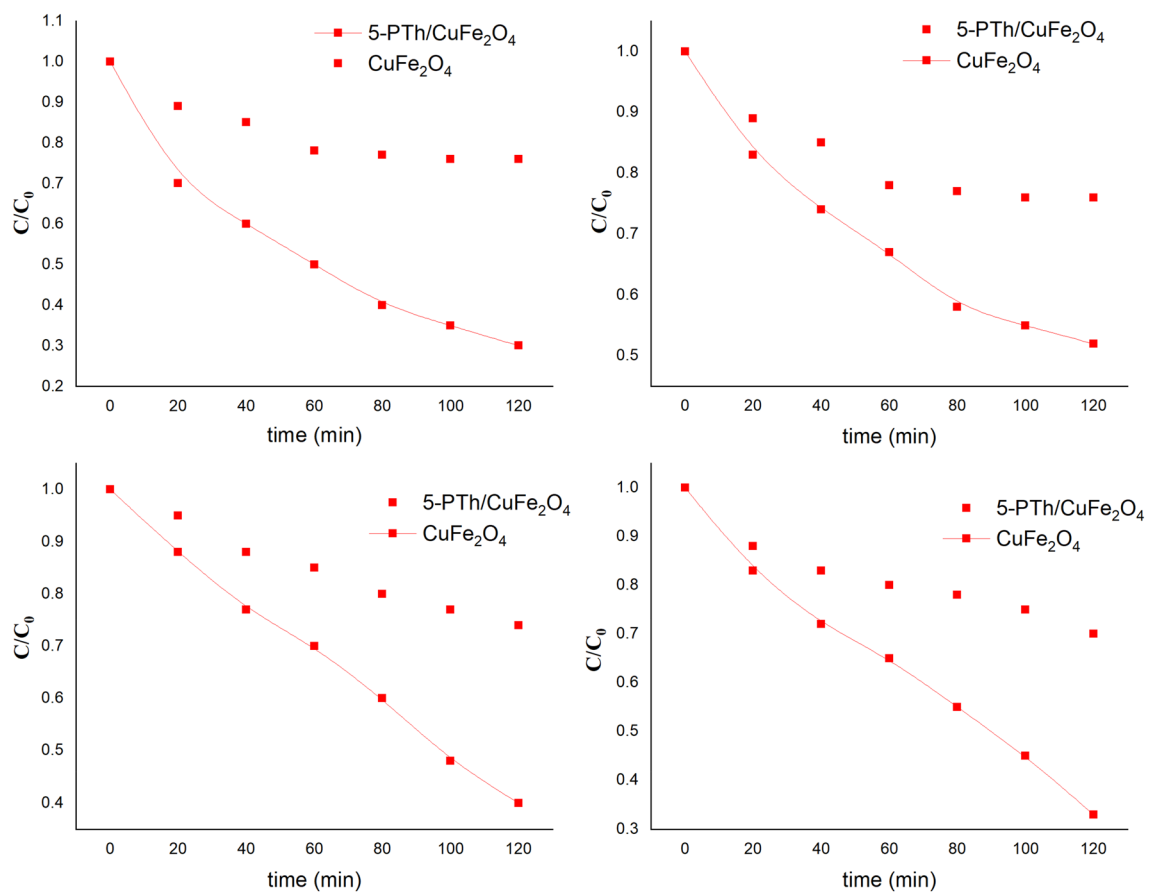


Figure 6. Recyclability test using CuFe₂O₄ and 5-PTh/CuFe₂O₄.

recyclability tests showed that the photocatalyst could be safely used up to a maximum of four cycles. For the PE films, a maximum degradation of 50% was achieved under microwave irradiation for 5 h using 5-PTh/CuFe₂O₄ nanohybrid. The photocatalyst could be effectively used for visible light-induced degradation of pollutants as well as microwave-assisted degradation of polymers.

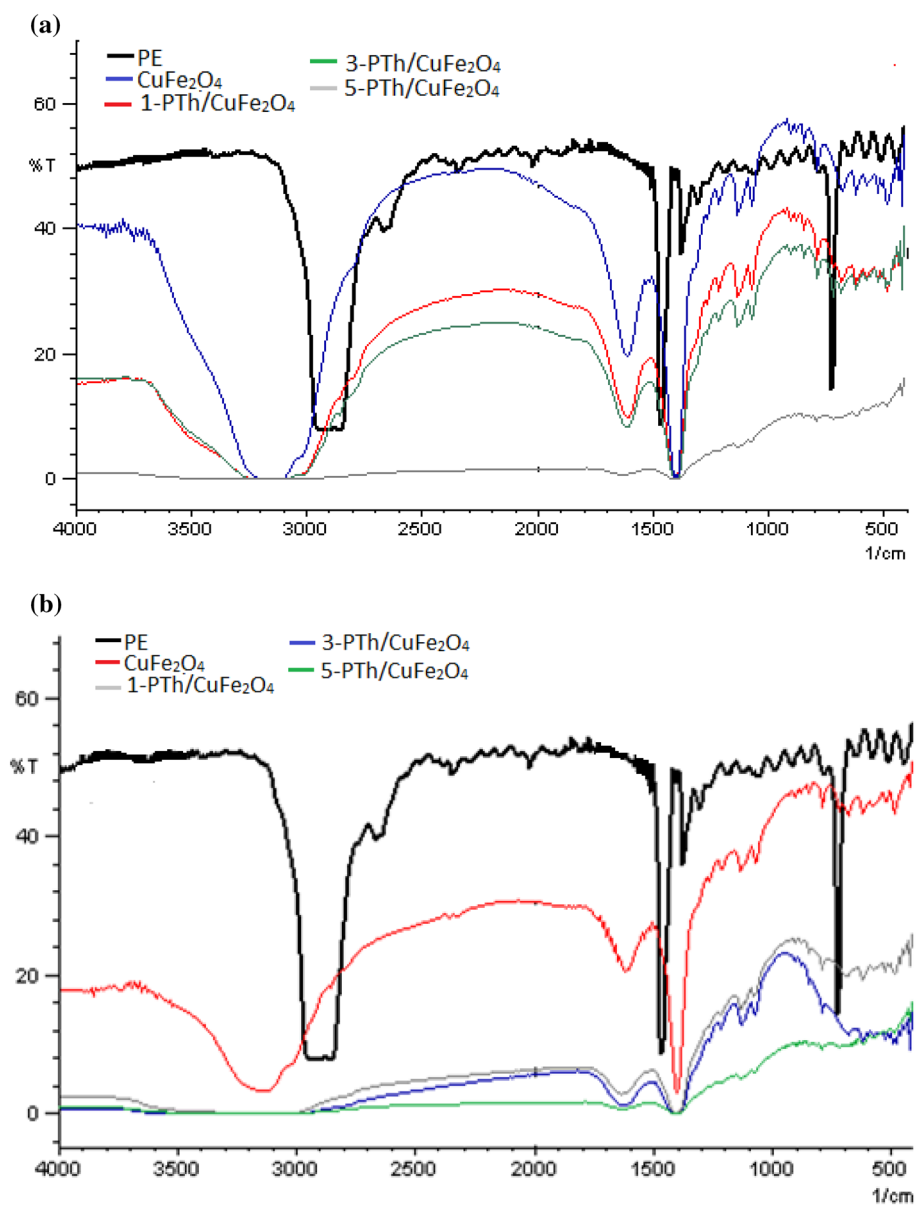


Figure 7. FTIR of (a) photo-catalytically degraded PE films (b) microwave degraded PE films.

Catalyst used	Initial weight (g)	Final weight (g) PE by photocatalysis	Final weight (g) PE microwave	% wt. loss PE by photocatalysis	% wt. loss PE by microwave
CuFe_2O_4	0.004 g	0.0036 g	0.0029 g	10%	27.5%
1-PTh/ CuFe_2O_4	0.004 g	0.0034 g	0.0027 g	15%	32.5%
3-PTh/ CuFe_2O_4	0.004 g	0.0032 g	0.0024 g	20%	40%
5-PTh/ CuFe_2O_4	0.004 g	0.0031 g	0.0020 g	22.5%	50%

Table 1. Percentage of weight loss in degraded PE via photocatalysis and microwave degradation.

Data availability

All data generated or analysed during this study are included in this published article [and its supplementary information files.

Received: 23 December 2022; Accepted: 28 February 2023

Published online: 27 March 2023

References

1. <http://worldcommoditytraders.com>.
2. Chen, W. *Inorganic Chemical Technology* 285–287 (Chemical Industry Press, 2002).
3. Landis, N. J. *Urea hydrolysis, US Patent 4341640* (1982).
4. Rahimpour, M. R. A non-ideal rate-based model for industrial urea thermal hydrolyser. *Chem. Eng. Process* **43**, 1299–1307 (2004).
5. Campos, J. L., Sanchez, M., Mosquera-Corral, A., Mendez, R. & Lema, J. M. Coupled BAS and anoxic USB system to remove urea and formaldehyde from wastewater. *Water Res.* **37**, 3445–3451 (2003).
6. Hoque, M. A. & Aravinthan, V. Modeling urea biodegradation in activated sludge using combined respirometric–titrimetric measurements. *Desalin. Water Treat.* **32**, 115–125 (2011).
7. Deng, Y., Zhang, Y. & Lemos, B. Tissue accumulation of microplastics in mice and biomarker responses suggest widespread health risks of exposure. *Sci. Rep.* **7**, 46687 (2017).
8. Wright, S. L., Thompson, R. C. & Galloway, T. S. The physical impacts of microplastics on marine organisms: A review. *Environ. Pollut.* **178**, 483–492 (2013).
9. Brandts, I. *et al.* Effects of nanoplastics on *Mytilus galloprovincialis* after individual and combined exposure with carbamazepine. *Sci. Total Environ.* **643**, 775–784 (2018).
10. George, S., Chellapandian, M., Sivasankar, B. & Jayaraman, K. A new process for the treatment of fertilizer effluent using immobilized urease. *Bioprocess. Eng.* **16**, 83–85 (1997).
11. Paço, A. *et al.* Biodegradation of polyethylene microplastics by the marine fungus *Zalerion maritimum*. *Sci. Total Environ.* **586**, 10–15 (2017).
12. Alia, S. S. *et al.* Photocatalytic degradation of low density polyethylene (LDPE) films using titania nanotubes. *Environ. Nanotech. Mon. Manag.* **5**, 44–53 (2016).
13. Tofa, T. S., Kunjali, K. L., Paul, S. & Dutta, J. Visible light photocatalytic degradation of microplastic residues with zinc oxide nanorods. *Environ. Chem. Lett.* **17**, 1341–1346 (2019).
14. Gonzalez, E. I. C. Microplastic pollution reduction by a carbon and nitrogen-doped TiO₂: Effect of pH and temperature in the photocatalytic degradation process. *J. Hazard. Mater.* **395**(5), 122632 (2020).
15. Tarazona, M. C. A., Chiu, J. F. V., Barbieri, V., Siligardi, C. & Gonzalez, E. I. C. New strategy for microplastic degradation: Green photocatalysis using a protein-based porous N-TiO₂ semiconductor. *Ceram. Int.* **45**(7), 9618–9624 (2019).
16. Tofa, T. S., Ye, F., Kunjali, K. L. & Dutta, J. Enhanced visible light photodegradation of microplastic fragments with plasmonic platinum/zinc oxide nanorod photocatalysts. *Catalysts* **9**(10), 819 (2019).
17. Klein, S., Dimzon, I. K., Eubeler, J. & Knepper, T. P. Analysis, occurrence, and degradation of microplastics in the aqueous environment. *Freshw. Microplast.* **1**, 51–67 (2018).
18. Gibson, M. A. & Hightower, J. W. Oxidative dehydrogenation of butenes over magnesium ferrite kinetic and mechanistic studies. *J. Catal.* **41**, 420–430 (1976).
19. Manova, E. *et al.* Mechanochemically synthesized nano-dimensional iron–cobalt spinel oxides as catalysts for methanol decomposition. *Appl. Catal. A* **277**, 119–127 (2004).
20. Paldey, S., Gedevisanishvili, S., Zhang, W. & Rasouli, F. Evaluation of a spinel based pigment system as a CO oxidation catalyst. *Appl. Catal. B* **56**, 241–250 (2005).
21. Zia, J., Aazam, E. S. & Riaz, U. Facile synthesis of MnO₂ nanorods and ZnMn₂O₄ nanohexagons: A comparison of microwave-assisted catalytic activity against 4-nitrophenol degradation. *J. Mater. Res. Technol.* **9**(5), 9709–9719 (2020).
22. Zia, J. & Riaz, U. Studies on the spectral, morphological and magnetic properties of PCz-PPy copolymer encapsulated BaFe₂O₄ nanohybrids. *J. Mater. Sci. Mater. Electr.* **31**, 22856–22865 (2020).
23. Zia, J., Farhat, S. M., Aazam, E. S. & Riaz, U. Highly efficient degradation of metronidazole drug using CaFe₂O₄/PNA nanohybrids as metal-organic catalysts under microwave irradiation. *Environ. Sci. Pollut. Res.* **28**, 4125–4135 (2021).
24. Riaz, U., Ashraf, S. M., Raza, R., Kohli, K. & Kashyap, J. Sonochemical facile synthesis of self-assembled poly(*o*-phenylenediamine)/cobalt ferrite nanohybrid with enhanced photocatalytic activity. *Ind. Eng. Chem. Res.* **55**(22), 6300–6309 (2016).
25. Kashyap, J., Gautam, S., Ashraf, S. M. & Riaz, U. Synergistic performance of sonolytically synthesized poly(1-naphthylamine)/TiO₂ nanohybrids: Degradation studies of amido black-10B Dye. *Chem. Select* **3**(42), 11926–11934 (2018).
26. Zia, J., Ajeer, M. & Riaz, U. Visible-light driven photocatalytic degradation of Bisphenol-a using ultrasonically synthesized polypyrrole/K-birnessite nanohybrids: experimental and DFT studies. *J. Environ. Sci.* **79**, 161–173 (2019).
27. Riaz, U., Ashraf, S. M. & Aqib, M. Microwave-assisted degradation of acid orange using a conjugated polymer, polyaniline, as catalyst. *Arab. J. Chem.* **7**(1), 79–86 (2014).
28. Zia, J., Fatima, F. & Riaz, U. A comprehensive review on the photocatalytic activity of polythiophene-based nanocomposites against degradation of organic pollutants. *Catal. Sci. Technol.* **11**, 6630–6648 (2021).
29. Venkatramana, C., Botsa, S. M., Shyamala, P. & Muralikrishna, R. Photocatalytic degradation of polyethylene plastics by NiAl₂O₄ spinels-synthesis and characterization. *Chemosphere* **265**, 129021 (2021).
30. Quyang, Z. *et al.* Recent advances in photocatalytic degradation of plastics and plastic-derived chemicals. *J. Mater. Chem. A* **9**, 13402–13441 (2021).
31. Riaz, U. & Zia, J. Microwave-assisted rapid degradation of DDT using nanohybrids of PANI with SnO₂ derived from Psidium Guajava extract. *Environ. Pollut.* **259**, 113917 (2020).
32. Zia, J., Kashyap, J. & Riaz, U. Facile synthesis of polypyrrole encapsulated V₂O₅ nanohybrids for visible light driven green sono-photocatalytic degradation of antibiotics. *J. Mol. Liq.* **272**, 834–850 (2018).
33. Amir, M. *et al.* Mossbauer studies and magnetic properties of cubic CuFe₂O₄ nanoparticles. *J. Supercond. Magn* **32**, 557–564 (2019).
34. Humbe, A. V., Kounsalye, J. S., Somvanshi, S. B., Kumar, A. & Jadhav, K. M. Cation distribution, magnetic and hyperfine interaction studies of Ni–Zn spinel ferrites: Role of Jahn Teller ion (Cu²⁺) substitution. *Mater. Adv.* **1**, 880–890 (2020).
35. Somvanshi, S. B., Khedkar, M. V., Kharat, P. B. & Jadhav, K. M. Influential diamagnetic magnesium (Mg²⁺) ion substitution in nano-spinel zinc ferrite (ZnFe₂O₄): Thermal, structural, spectral, optical and physisorption analysis. *Ceram. Int.* **46**(7), 8640–8650 (2020).
36. Wu, L. K. *et al.* Highly porous copper ferrite foam: A promising adsorbent for efficient removal of As(III) and As(V) from water. *J. Hazard. Mater.* **347**, 15–24 (2021).
37. D’Amelia, R. P., Gentile, S., Nirode, W. F. & Huang, L. Quantitative analysis of copolymers and blends of polyvinyl acetate (PVAc) using Fourier transform infrared spectroscopy (FTIR) and elemental analysis (EA). *World J. Chem. Edu.* **4**(2), 25–31 (2016).

Acknowledgements

The authors wish to acknowledge National Science Foundation (Award # 2122044), the NSF PREM for Hybrid Nanoscale Systems between NCCU and Penn State for providing financial assistance.

Author contributions

U.R. wrote the manuscript, S.G. carried out the synthesis of the nanohybrid, K.H. compiled the degradation studies, F.Y. helped with the LCMS studies and analysis.

Competing interests

The authors declare no competing interests.

Additional information

Supplementary Information The online version contains supplementary material available at <https://doi.org/10.1038/s41598-023-30669-x>.

Correspondence and requests for materials should be addressed to U.R.

Reprints and permissions information is available at www.nature.com/reprints.

Publisher's note Springer Nature remains neutral with regard to jurisdictional claims in published maps and institutional affiliations.



Open Access This article is licensed under a Creative Commons Attribution 4.0 International License, which permits use, sharing, adaptation, distribution and reproduction in any medium or format, as long as you give appropriate credit to the original author(s) and the source, provide a link to the Creative Commons licence, and indicate if changes were made. The images or other third party material in this article are included in the article's Creative Commons licence, unless indicated otherwise in a credit line to the material. If material is not included in the article's Creative Commons licence and your intended use is not permitted by statutory regulation or exceeds the permitted use, you will need to obtain permission directly from the copyright holder. To view a copy of this licence, visit <http://creativecommons.org/licenses/by/4.0/>.

© The Author(s) 2023